

Evolution Dynamics Toward the Limit Cycle of a Quantum Self-Sustained Oscillator

Hendry Minfui Lim,^{1,2,*} Donny Dwiputra,^{3,2,†} M Shoufie Ukhtary,^{2,‡} and Ahmad R. T. Nugraha^{2,4,5,§}

¹*Department of Physics, Faculty of Mathematics and Natural Sciences, Universitas Indonesia, Depok 16424, Indonesia*

²*Research Center for Quantum Physics, National Research and Innovation Agency (BRIN), South Tangerang 15314, Indonesia*

³*Asia Pacific Center for Theoretical Physics, Pohang 37673, Korea*

⁴*Research Collaboration Center for Quantum Technology 2.0, Bandung 40132, Indonesia*

⁵*Department of Engineering Physics, Telkom University, Bandung 40257, Indonesia*

(Dated: June 27, 2024)

The dynamics of a quantum self-sustained oscillator as it evolves toward its limit cycle may be useful in solving related problems like those in quantum synchronization, yet is inadequately studied. Here we investigate the evolution of a quantum Rayleigh-van der Pol (RvdP) oscillator, the simplest form of a self-sustained oscillator exhibiting a quasiharmonic limit cycle, starting from Fock, thermal, and coherent states. We find that the phase-space dynamics significantly differ depending on the initial state—one evolution toward the limit cycle may take much longer than another and a least-time parameter may be present. We describe the resulting dynamics in terms of the coherence decay and the redistribution of eigenstate occupation.

When subjected to a sufficiently weak, uni- or bi-directional coupling to one another, two or more oscillators may progressively match their rhythms to become synchronized—being under either frequency or phase entrainment [1, 2]. Synchronization is ubiquitous in nature—the circadian rhythm driven by external light [3, 4], flashing of bioluminescent insects [5, 6], a Belousov–Zhabotinsky reaction under light pulses [7], and a laser network [8], to name a few—and it serves as a key mechanism in establishing order out of disorder in complex systems [9–11]. For synchronization to occur, an oscillator must have its own rhythm—the self-sustaining property is necessary for synchronization. A self-sustained oscillator is characterized by at least one source of energy dissipation (damping) and energy pump, such that there is a dynamical equilibrium between the opposing forces. This requires nonlinearities to be present in the system. In the phase space representation of the oscillator, the equilibrium corresponds to a limit cycle to which an arbitrary phase point is always attracted [1, 2]. The form of the limit cycle depends on the mathematical description of the system [12, 13]. Multiple limit cycles can exist for a more complex system [14]. Additional examples of self-sustaining oscillators include wall clocks, electronic systems [15], circadian rhythms [16, 17], chemical reactions [18, 19], and predator-and-prey systems [20].

The quantum version of self-sustained oscillators has been gaining interest in recent years. One distinct feature of quantum self-sustained oscillators is the smearing of the limit cycle due to quantum noise [21]. Typical mathematical descriptions use the Lindblad master equation [22–39], although different formalism is possible [40]. Recent research involving quantum self-sustained oscillators is mostly concerned with quantum synchronization, such as quantum synchronization under external driving [25–30, 38], squeezing [30, 31], and coupling to other oscillators [32–39]. Intriguing results were found about

quantum frequency or phase entrainment, quantum fluctuations [27, 34], critical response [28], information measures [30], classicality [30, 31, 35], entanglement [33], and amplitude death or oscillation collapse [36–38]. Several studies also proposed quantifying the degree of quantum synchronization [41–44]. Furthermore, research has been done to speed up synchronization via drive engineering [45]. Apart from quantum synchronization, quantum limit cycles also play an important role in heat engines [22, 23] and single-electron transistors [24].

Similar to quantum synchronization, prior studies on the dynamics of quantum self-sustained oscillators are mainly concerned with the steady-state dynamics—the limit cycles—apart from the foundational work of quantizing the equations of motion [21, 26]. The full dynamics toward the quantum limit cycle are much less explored. Unlike the classical case, the motion of the phase point attracted to the limit cycle is not the only information to obtain. In the quantum case, the expected phase point does not contain all the information about the motion we may extract from the phase-space representation. It is also interesting to track how quantum features, such as quantum coherence, change along the evolution. Such information might be useful in solving related problems like those in quantum synchronization. This motivates us to study how a quantum self-sustained oscillator evolves from a given initial state toward its limit cycle, and how the processes in the system affect the dynamics.

In this Letter, we study the dynamics of the simplest form of a quantum self-sustained oscillator: the quantum Rayleigh-van der Pol (RvdP) oscillator. The simplicity lies in the fact that its limit cycle is circular, making it quasiharmonic. Despite its simplicity, the system can be physically realized with a cavity optomechanical system [25, 32] and trapped ions [34]. We study the system’s evolution starting as a Fock state, a thermal state, and a coherent state. We observe that the evolution is similar for the Fock and thermal states, but largely different for

the coherent state. In particular, we find that for a given Fock state and thermal state, there is a set of parameters for which the limit cycle is reached with the least amount of time. In addition to that, we observe that the limit cycle is reached in a much longer time when the oscillator evolves from the coherent state. This may be attributed to the longer time it takes for the coherence between neighboring eigenstates of the system to vanish.

Depending on how the equation of motion is quantized, the resulting quantum equation of motion of a self-sustained oscillator may deviate from the classical counterpart when some parameters are not small [21]. With more careful consideration, an exact but more complicated quantum model may be obtained [26]. Our mathematical model adopts the one used by Ben Arosh et al. [21] and is given by the following dimensionless Lindblad's master equation (with $\hbar = 1$):

$$\dot{\rho} = -i [\hat{a}^\dagger \hat{a}, \rho] + \kappa_1 \mathcal{D} [\hat{a}^\dagger] \rho + \gamma_1 \mathcal{D} [\hat{a}] \rho + \gamma_2 \mathcal{D} [\hat{a}^2] \rho, \quad (1)$$

where $\hat{a} = (\hat{x} + i\hat{p})/\sqrt{2}$ and $\mathcal{D} [\hat{O}] \rho = \hat{O} \rho \hat{O}^\dagger - (1/2) \{ \hat{O}^\dagger \hat{O}, \rho \}$. In Eq. (1), the time is measured in units of the oscillator's natural frequency ω_0 (making the simple harmonic period 2π), mass is in terms of the oscillator's mass m , and length is in units of $\sqrt{\hbar/m\omega_0}$. Contrary to what it is usually called [25, 28, 31–37, 39], this equation does not describe the van der Pol (vdP) oscillator since its steady-state Wigner function has a parameter-independent radial symmetry—a feature not present in a vdP oscillator [21]. There are three sources of non-conservative mechanisms responsible for the self-sustaining property: κ_1 parameterizes the rate of one-quantum pump, γ_1 parameterizes the rate of one-quantum dissipation, and γ_2 parameterizes the rate of two-quantum dissipation.

We provide a brief overview of properties described by Ben Arosh et al. [21] that are useful in our analysis. Equation (1) approximates the classical counterpart:

$$\ddot{x} + x - [\kappa_1 - \gamma_1 - \gamma_2 (x^2 + \dot{x}^2)] \dot{x} = 0, \quad (2)$$

with an error $\mathcal{O}((\kappa_1 - \gamma_1)^2)$, meaning that the oscillator is not an exact quantization of the RvdP oscillator. The steady-state Wigner function describing the limit cycle takes the form of a ring uniformly smeared out around a circle centered at the origin, with radius $\sqrt{(\kappa_1 - \gamma_1)/\gamma_2}$. The radial symmetry of the steady-state Wigner function implies that the steady-state density matrix—obtained by setting the left-hand side of Eq. (1) to zero—is diagonal. This means that the system always evolves toward being a statistical mixture, losing all of its quantum coherence. Lastly, it is more convenient to analyze the system's evolution by considering the evolution of the elements along each “off-diagonal” (not in the usual sense

of the word—we drop the quotation marks for the remainder of this text) of the density matrix. We use the following transformation:

$$\sigma_{nm}(t) = e^{-imt} \sqrt{\frac{(n+m)!}{n!}} \rho_{n,n+m}, \quad (3)$$

where $m + n \geq 0$. The quantity σ_{nm} defines the element indexed n along the m th off-diagonal. Taking the evolution of the density matrix elements ρ_{jk} from Eq. (1), then applying this transformation, we obtain

$$\begin{aligned} \dot{\sigma}_{nm} = & \kappa_1 \left[(n+m) \sigma_{n-1,m} - \frac{1}{2} (2n+m+2) \sigma_{nm} \right] \\ & + \gamma_1 \left[(n+1) \sigma_{n+1,m} - \frac{1}{2} (2n+m) \sigma_{n,m} \right] \\ & + \gamma_2 \left[(n+1)(n+2) \sigma_{n+2,m} \right. \\ & \left. - \frac{1}{2} [(n-1)n + (n+m-1)(n+m)] \sigma_{n,m} \right]. \end{aligned} \quad (4)$$

Equation (4) shows that a given density matrix element is only coupled to the others in the same off-diagonal. Since the steady-state density matrix is diagonal, we can deduce that all $m \neq 0$ off-diagonals undergo decay, while the diagonal elements redistribute themselves.

The radial symmetry of the quantum limit cycle—represented by the steady-state Wigner function—means that the expected position and momentum of the system are zero. However, the quantum limit cycle indeed contains information about these quantities [26], albeit only qualitatively due to the quasi-probabilistic nature of the Wigner function. The peak of the quantum limit cycle, which coincides with the classical limit cycle, gives the most probable limit cycle of the system. Meanwhile, the smearing around the circle represents other limit cycles deviating from the classical case, that may be observed with lower probabilities.

We numerically simulate the system's evolution from a Fock, thermal, and coherent state. These states are chosen due to their simplicity and peculiarities: the Fock state is the energy eigenstate; the thermal state is a mixed state corresponding to thermal equilibrium; and the coherent state is a pure state that behaves similarly to a classical oscillator. Since the evolution involves pumping and dissipation of quanta of energy, we choose the initial states with the same initial values for the expected number $\langle n \rangle = \langle \hat{a}^\dagger \hat{a} \rangle$ of excitation, which we denote $\langle n \rangle_0$ herein. We study the evolution of the Wigner function [46]

$$W(x, p, t) = \frac{1}{2\pi} \int_{-\infty}^{\infty} \left\langle x - \frac{y}{2} \left| \rho(t) \right| x + \frac{y}{2} \right\rangle e^{ipy} dy$$

to provide a direct comparison to the classical phase space motion. Since the peak of a coherent state moves in

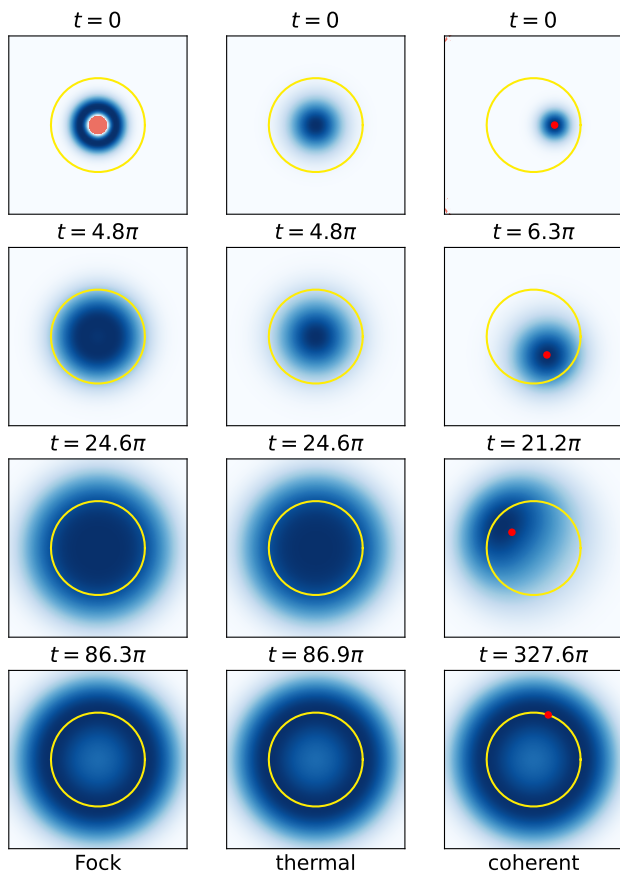


FIG. 1. Wigner function evolution snapshots of the quantum RvdP oscillator for different initial states in the weakly nonlinear regime with $\kappa_1 = 0.1, \gamma_1 = 0.09, \gamma_2 = 0.001$. The same color values correspond to different Wigner function values between the plots—this is done to emphasize the maximum of the Wigner functions. Negative Wigner function values (only at the central region of the top-left plot) are colored pale red. The snapshots showcase significant stages of the evolution toward the limit cycle, with the bottom row showing the Wigner functions reaching their steady states. The yellow circle is the classical limit cycle while the red point in the plots for the coherent state is the classical phase point at the given time. The initial states have $\langle n \rangle = 1$. One simple harmonic period is 2π under the specified unit system.

the same way a classical phase point moves in the phase space, we additionally track the motion of the peak of the Wigner function for the coherent state case and simulate Eq. (2) starting at the initial expected phase point of the quantum states. The simulation is done for the weakly nonlinear and the strongly nonlinear case. We keep the parameter difference ($\kappa_1 - \gamma_1$) small so that the system describes an RvdP oscillator as closely as possible.

Figures 1 and 2 show selected evolution snapshots for different initial states with $\langle n \rangle_0 = 1$, for the weakly and strongly nonlinear regimes, respectively. Our analysis uses the terms “Wigner function” and “occupation probability distribution” (ρ_{jj} versus j) frequently, so we shall

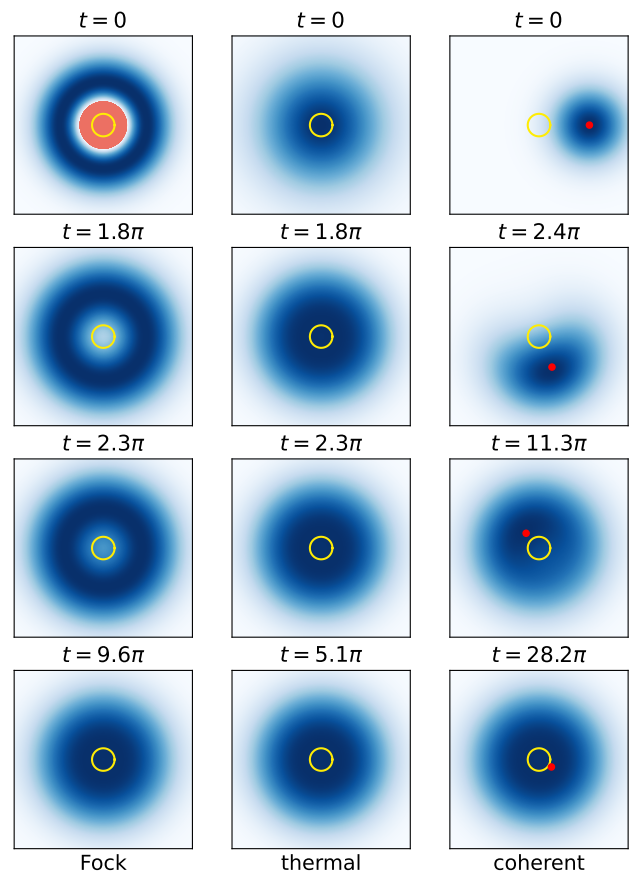


FIG. 2. Same as Fig. 1 but in the strongly nonlinear regime with $\kappa_1 = 0.1, \gamma_1 = 0.09, \gamma_2 = 0.1$. The plots are zoomed in for better visibility.

refer to them as “WF” and “OPD” for brevity and clarity. We do not plot the OPD as the information we need may be straightforwardly extracted from the WF.

For the Fock state case in the weakly nonlinear regime, the WF approaches a nonnegative distribution and smears out radially as the OPD gains a finite width. It then continues to smear as the width of the OPD increases, similar to how a thermal state’s WF is more smeared out and its OPD’s width becomes larger with increasing $\langle n \rangle$. Finally, the WF approaches the steady-state distribution by losing value at the central region as the occupations in the first few lowest levels go down. The WF keeps its radial symmetry all the time as the off-diagonal elements are always zero. This can be seen from Eq. (4) for any $m \neq 0$, noting that the density matrix is initially diagonal. In the strongly nonlinear regime, we observe the WF clumping radially instead of smearing, indicating that the OPD shifts toward lower eigenenergies due to the strong nonlinear energy dissipation.

A thermal state undergoes a similar evolution, except without the Fock state case’s first stage since a thermal state’s WF is nonnegative and its OPD has a finite width, to begin with. The similarity between these two cases is

to be expected: the density matrix is always diagonal and only undergoes diagonal element redistribution with the same set of parameters. Over the late evolution, the WF in both cases for a given time become closely similar to each other, as shown in the bottom two rows of the figures.

A coherent state evolves in a largely different manner, due to the presence of $m \neq 0$ off-diagonal elements and hence coherence decay, in addition to diagonal element redistribution. In this case, we observe a rotation of period 2π about the origin in the phase space at uniform speed, similar to the classical case, as the WF radially approaches the limit cycle radius. However, the classical phase point at any given time does not always coincide with the WF maximum as the evolution proceeds. This can be most easily seen in the third-row plot for the coherent state case in Fig. 1. We observe the WF smearing angularly in addition to smearing radially, which shows that the system gradually loses its phase. It is noteworthy that our observation here does not agree with the description of Ben Arosh et al. [21] that the Wigner function reaches the limit cycle first and then starts to lose its phase. We shall not describe the result for this case in terms of the OPD since the WF is also influenced by the $m \neq 0$ elements, making the relation between OPD and the form of the WF more complicated.

The bottom rows of Figs. 1 and 2 show the Wigner function at approximately the time when the system reaches the limit cycle. We define the steady-state time T_{ss} as the time it takes the system to be sufficiently close to the steady state (i.e. the limit cycle). We use the trace distance [47] as our distance measure, and our criterion for T_{ss} is that

$$d_{\text{Tr}}(\rho(T_{ss}), \rho_{ss}) = \frac{1}{2} \text{Tr} \{ |\rho(T_{ss}) - \rho_{ss}| \} < \epsilon, \quad (5)$$

where $|A| = \sqrt{A^\dagger A}$, for some small ϵ which we choose to be 10^{-3} . We observe that T_{ss} for a given initial state is smaller in the strongly nonlinear regime. In particular, it takes significantly longer for the coherent state to reach the limit cycle than the Fock state and the thermal state. Intriguingly, for the Fock state and the thermal state, T_{ss} is approximately the same in the weakly nonlinear regime but is significantly different in the strongly nonlinear regime. This suggests that the dependence of the steady-state time on the nonlinearity is not trivial. To reveal this dependence, we numerically calculate T_{ss} as a function of increasing nonlinearities, with several values of $\langle n \rangle_0$ as an additional parameter for comparison.

Figure 3 shows the dependence of T_{ss} on nonlinearity with the two previous cases as the extremes. T_{ss} is similar between the Fock and thermal state case for the given $\langle n \rangle_0$, decreasing with increasing nonlinearity except over an interval where T_{ss} dips down before going back up. The nonlinearity at which this dip occurs differs between the Fock and thermal state cases and tends toward the

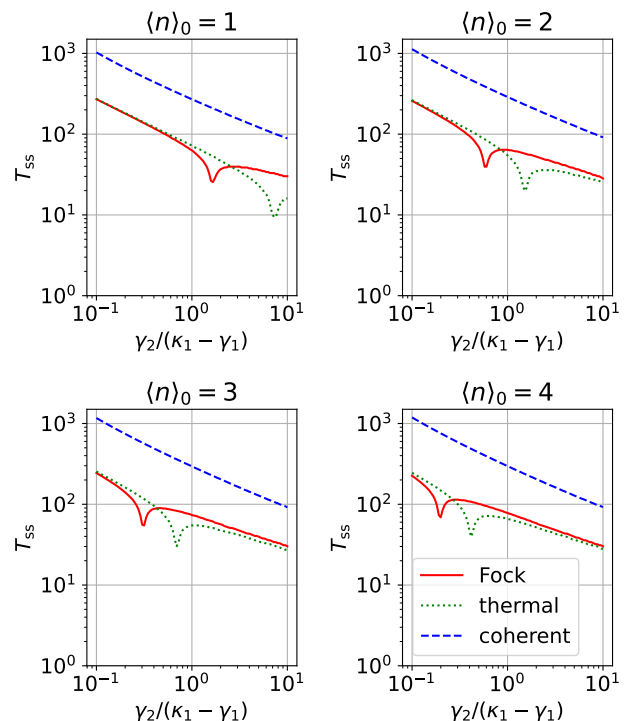


FIG. 3. Time T_{ss} required to reach the steady-state limit cycle as a function of nonlinearity quantified by $\gamma_2/(\kappa_1 - \gamma_1)$, recorded as the trace distance to the steady-state density matrix falls below 10^{-3} . Here $\kappa_1 = 0.1, \gamma_1 = 0.09$. Each plot shows the simulation result for initial states with different expected numbers $\langle n \rangle_0$ of excitation. In particular, the first and last points of the lines in the top left panel give the steady-state time for the evolution depicted in Figs. 1 and 2, respectively. The value for a given initial state with a given nonlinearity shows no particular trend with increasing $\langle n \rangle_0$ —it may increase, decrease, or fluctuate.

weak-nonlinearity side as $\langle n \rangle_0$ increases. Additionally, we observe a larger dip in the thermal state case. The presence of these dips shows that there is one set of parameters that is the most favorable for the Fock/thermal state with a given $\langle n \rangle_0$ to reach the steady-state OPD. We observe no simple trend with increasing $\langle n \rangle_0$ —for a given $\gamma_2/(\kappa_1 - \gamma_1)$ the calculated T_{ss} for either state may increase, decrease, or fluctuate with increasing $\langle n \rangle_0$. The coherent state case generally takes significantly longer to reach the limit cycle. The T_{ss} behavior is also different from the other two cases. Here, we observe a steady decrease in T_{ss} with increasing nonlinearity. We also observe that T_{ss} increases with $\langle n \rangle_0$. The amount by which T_{ss} increases gets smaller as the nonlinearity gets stronger.

Finally, we investigate the reason behind the long T_{ss} in the coherent state case. One obvious clue is the presence of nonzero $m \neq 0$ off-diagonal elements. As observed in Figs. 1 and 2, the system takes a large amount

of time to become radially uniform, which means that the $m \neq 0$ off-diagonal terms have not completely decayed. However, it is not obvious whether the OPD is already stationary at the time. Lead by this, we investigate the difference in timescale between the coherence decay and the diagonal-element redistribution by numerically calculating the time it takes for the density matrix elements to reach their steady-state values, i.e. for the diagonal elements to reach the steady-state distribution and the off-diagonal elements to vanish. We numerically calculate the distance of the m th off-diagonal from its steady-state value:

$$d_m = \sum_n \left| \rho_{n,n+m}(t) - \rho_{n,n+m}^{(ss)} \right|, \quad (6)$$

where $n+m \geq 0$. We note that it is also valid to use the transformed elements σ_{nm} instead of the true elements $\rho_{n,n+m}$. As the strength of the nonlinearity does not qualitatively change the evolution of the system (compare Fig. 1 and Fig. 2), we arbitrarily choose the strongly nonlinear regime with the same parameters as that resulting in Fig. 2 for the coherent state case. This allows us to conveniently truncate the Hilbert space dimension at some low value N , for which $|m| < N$.

Figure 4 shows our calculation result for $0.1 \leq t \leq T_{ss}$. The diagonal elements (labeled “ $m = 0$ ”) reach their steady-state distribution at approximately the same time the $m = \pm 2$ off-diagonals vanishes. At this time, the $m = \pm 1$ off-diagonals have not vanished and they are the last to reach their steady-state values. Thus, the long T_{ss} may be attributed to the slowness of the decay of the coherence between the n th and the $(n \pm 1)$ th eigenstates. We further note that the non-diagonal-element decay

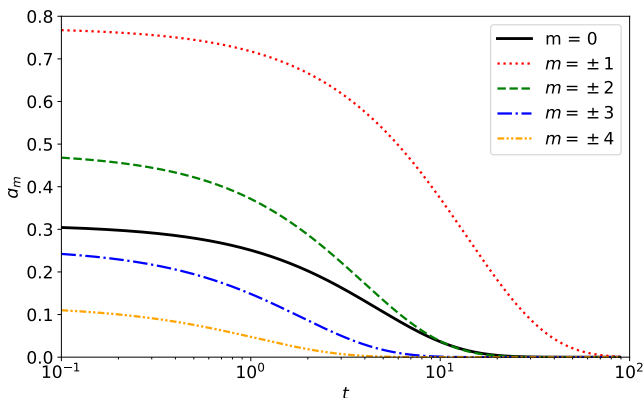


FIG. 4. Distance between the m th off-diagonal from its steady state, as defined in Eq. (6). A truncated Hilbert space of dimension $N = 12$ is used, meaning that $|m| < 12$. The rest of the lines are omitted as they start small and decay quickly, cluttering the bottom left part of the plot. The calculation is performed in the strongly nonlinear regime with $\kappa_1 = 0.1, \gamma_1 = 0.09, \gamma_2 = 0.1$, initialized as a coherent state with $\langle n \rangle_0 = 1$.

rate is lower for larger m —the $m = \pm 1$ off-diagonals take longer to decay because the initial values are larger. Based on what we observe in Fig. 4, we predict that below certain initial values of the off-diagonal elements, the one to determine T_{ss} will be the time it takes to reach the steady-state ODP instead. This may be the case for other initial states that we do not discuss here, such as some superposition of Fock states.

In conclusion, we have studied the evolution dynamics of a quantum Rayleigh-van der Pol (RvdP) oscillator initialized as a Fock, thermal, and coherent state. We have observed that the evolution is different depending on the existence of off-diagonal elements of the density matrix. We have found that for a coherent state, the coherence between neighboring eigenstates of the system takes a longer time to completely decay compared to the time it takes for the diagonal elements to reach the steady-state distribution, leading to significantly longer steady-state time compared to a fock and thermal state. We have also found that for a given Fock or thermal state, there is a set of oscillator parameters for which it reaches the limit cycle in the least amount of time. Our findings contribute to a further understanding of the dynamics of the RvdP oscillator and might be useful in solving related problems such as quantum synchronization. For example, it might be possible to speed up synchronization involving coherent states by finding a way to speed up the coherence decay or to speed up synchronization involving Fock/thermal states by utilizing the least-time parameters.

We thank the Mahameru BRIN High-Performance Computing for their HPC facilities. We acknowledge the use of the following Python packages: NumPy [48], SciPy [49], QuTiP [50, 51], and Matplotlib [52]. H. M. L. is supported by Indonesia’s National Research and Innovation Agency’s National Talent Management System Research Assistantship Fund. The data supporting the findings of this study are available from the corresponding authors, upon reasonable request.

* Author to whom correspondence should be addressed: hendry01@ui.ac.id

† Author to whom correspondence should be addressed: donny.dwiputra@apctp.org

‡ msho001@brin.go.id

§ ahma080@brin.go.id

- [1] A. Pikovsky, M. Rosenblum, and J. Kurths, *Synchronization: A Universal Concept in Nonlinear Sciences* (Cambridge University Press, 2001).
- [2] A. Balanov, N. Janson, D. Postnov, and O. Sosnovtseva, *Synchronization: From Simple to Complex* (Springer Berlin Heidelberg, 2008).
- [3] C. A. Czeisler, J. F. Duffy, T. L. Shanahan, E. N. Brown, J. F. Mitchell, D. W. Rimmer, J. M. Ronda, E. J. Silva, J. S. Allan, J. S. Emens, D.-J. Dijk, and R. E. Kronauer,

- Science **284**, 2177 (1999).
- [4] A. Ramkisoensing and J. H. Meijer, *Front. Neurol.* **6**, 00128 (2015).
- [5] J. Buck and E. Buck, *Sci. Am.* **234**, 74 (1976).
- [6] J. Buck and E. Buck, *Science* **159**, 1319 (1968).
- [7] A. L. Lin, M. Bertram, K. Martinez, H. L. Swinney, A. Ardelea, and G. F. Carey, *Phys. Rev. Lett.* **84**, 4240 (2000).
- [8] M. Nixon, M. Fridman, E. Ronen, A. A. Friesem, N. Davidson, and I. Kanter, *Phys. Rev. Lett.* **108**, 214101 (2012).
- [9] I. Blekhman, *J. Appl. Math. Mech.* **28**, 239 (1964).
- [10] E. Ott, *Chaos in dynamical systems* (Cambridge University Press, 2002).
- [11] A. C. Luo, *Commun. Nonlinear Sci. Numer. Simul.* **14**, 1901 (2009).
- [12] J.-H. He, *Chaos Solit. Fractals* **26**, 827 (2005).
- [13] Y. Ye, S. Cai, and C. Lo, *Theory of Limit Cycles* (American Mathematical Society, 1986).
- [14] C. Christopher, C. Li, and J. Torregrosa, *Limit Cycles of Differential Equations* (Springer International Publishing, 2024).
- [15] P. B. Reddy and I. A. Hiskens, in *2005 IEEE Russia Power Tech* (2005) p. 1.
- [16] M. E. Jewett, D. B. Forger, and R. E. Kronauer, *J. Biol. Rhythms* **14**, 493 (1999).
- [17] J.-C. Leloup, D. Gonze, and A. Goldbeter, *J. Biol. Rhythms* **14**, 433 (1999).
- [18] J. Schnakenberg, *J. Theor. Biol.* **81**, 389 (1979).
- [19] R. J. Field and R. M. Noyes, *J. Chem. Phys.* **60**, 1877 (1974).
- [20] K.-S. Cheng, *SIAM J. Math. Anal.* **12**, 541 (1981).
- [21] L. Ben Arosh, M. C. Cross, and R. Lifshitz, *Phys. Rev. Res.* **3**, 013130 (2021).
- [22] Y. Rezek and R. Kosloff, *New J. Phys.* **8**, 83 (2006).
- [23] T. Feldmann and R. Kosloff, *Phys. Rev. E* **70** (2004).
- [24] D. A. Rodrigues, J. Imbers, and A. D. Armour, *Phys. Rev. Lett.* **98**, 067204 (2007).
- [25] S. Walter, A. Nunnenkamp, and C. Bruder, *Phys. Rev. Lett.* **112**, 094102 (2014).
- [26] A. Chia, L. C. Kwek, and C. Noh, *Phys. Rev. E* **102**, 042213 (2020).
- [27] C. Navarrete-Benlloch, T. Weiss, S. Walter, and G. J. de Valcárcel, *Phys. Rev. Lett.* **119**, 133601 (2017).
- [28] S. Dutta and N. R. Cooper, *Phys. Rev. Lett.* **123**, 250401 (2019).
- [29] A. J. Sudler, J. Talukdar, and D. Blume, Driven generalized quantum rayleigh-van der pol oscillators: Phase localization and spectral response (2024), arXiv:2401.03823 [quant-ph].
- [30] S. Marti, U. von Lüpke, O. Joshi, Y. Yang, M. Bild, A. Omahen, Y. Chu, and M. Fadel, Quantum squeezing in a nonlinear mechanical oscillator (2023), arXiv:2312.16169.
- [31] S. Sonar, M. Hajdušek, M. Mukherjee, R. Fazio, V. Vedral, S. Vinjanampathy, and L.-C. Kwek, *Phys. Rev. Lett.* **120** (2018).
- [32] S. Walter, A. Nunnenkamp, and C. Bruder, *Ann. Phys.* **527**, 131 (2015).
- [33] T. E. Lee, C.-K. Chan, and S. Wang, *Phys. Rev. E* **89**, 022913 (2014).
- [34] T. E. Lee and H. R. Sadeghpour, *Phys. Rev. Lett.* **111**, 234101 (2013).
- [35] N. Lörch, E. Amitai, A. Nunnenkamp, and C. Bruder, *Phys. Rev. Lett.* **117**, 073601 (2016).
- [36] K. Ishibashi and R. Kanamoto, *Phys. Rev. E* **96**, 052210 (2017).
- [37] E. Amitai, M. Koppenhöfer, N. Lörch, and C. Bruder, *Phys. Rev. E* **97**, 052203 (2018).
- [38] Y. Shen, W.-K. Mok, C. Noh, A. Q. Liu, L.-C. Kwek, W. Fan, and A. Chia, *Phys. Rev. A* **107**, 053713 (2023).
- [39] C. Davis-Tilley, C. K. Teoh, and A. D. Armour, *New J. Phys.* **20**, 113002 (2018).
- [40] A. O. Bolivar, *Random Oper. and Stoch. Equ.* **9**, 275 (2001).
- [41] A. Mari, A. Farace, N. Didier, V. Giovannetti, and R. Fazio, *Phys. Rev. Lett.* **111**, 103605 (2013).
- [42] W. Li, W. Zhang, C. Li, and H. Song, *Phys. Rev. E* **96**, 012211 (2017).
- [43] N. Jaseem, M. Hajdušek, P. Solanki, L.-C. Kwek, R. Fazio, and S. Vinjanampathy, *Phys. Rev. Res.* **2**, 043287 (2020).
- [44] Y. Shen, H. Y. Soh, L.-C. Kwek, and W. Fan, *Entropy* **25**, 1116 (2023).
- [45] F. Impens and D. Guéry-Odelin, *Sci. Rep.* **13**, 1 (2023).
- [46] U. Leonhardt, *Measuring the Quantum State of Light* (Cambridge University Press, 1997).
- [47] M. A. Nielsen and I. L. Chuang, *Quantum Computation and Quantum Information: 10th Anniversary Edition* (Cambridge University Press, 2010).
- [48] C. R. Harris, K. J. Millman, S. J. van der Walt, R. Gommers, P. Virtanen, D. Cournapeau, E. Wieser, J. Taylor, S. Berg, N. J. Smith, R. Kern, M. Picus, S. Hoyer, M. H. van Kerkwijk, M. Brett, A. Haldane, J. F. del Río, M. Wiebe, P. Peterson, P. Gérard-Marchant, K. Sheppard, T. Reddy, W. Weckesser, H. Abbasi, C. Gohlke, and T. E. Oliphant, *Nature* **585**, 357 (2020).
- [49] P. Virtanen, R. Gommers, T. E. Oliphant, M. Haberland, T. Reddy, D. Cournapeau, E. Burovski, P. Peterson, W. Weckesser, J. Bright, S. J. van der Walt, M. Brett, J. Wilson, K. J. Millman, N. Mayorov, A. R. J. Nelson, E. Jones, R. Kern, E. Larson, C. J. Carey, Í. Polat, Y. Feng, E. W. Moore, J. VanderPlas, D. Laxalde, J. Perktold, R. Cimrman, I. Henriksen, E. A. Quintero, C. R. Harris, A. M. Archibald, A. H. Ribeiro, F. Pedregosa, P. van Mulbregt, and SciPy 1.0 Contributors, *Nat. Methods* **17**, 261 (2020).
- [50] J. Johansson, P. Nation, and F. Nori, *Comput. Phys. Commun.* **183**, 1760 (2012).
- [51] J. Johansson, P. Nation, and F. Nori, *Comput. Phys. Commun.* **184**, 1234 (2013).
- [52] J. D. Hunter, *Comput. Sci. Eng.* **9**, 90 (2007).